Microporous and Mesoporous Materials 185 (2014) 190–196

Contents lists available at ScienceDirect

Microporous and Mesoporous Materials

journal homepage: www.elsevier.com/locate/micromeso

Strong influence of the H_2 binding energy on the Maxwell–Stefan diffusivity in NU-100, UiO-68, and IRMOF-16

Yamil J. Colón [a], Rajamani Krishna [b,*], Randall Q. Snurr [a,*]

[a] Department of Chemical and Biological Engineering, Northwestern University, 2145 Sheridan Road, Evanston, IL 60208, USA
[b] Van 't Hoff Institute for Molecular Sciences, University of Amsterdam, Science Park 904, 1098 XH Amsterdam, The Netherlands

ARTICLE INFO

Article history:
Received 28 September 2013
Accepted 31 October 2013
Available online 9 November 2013

Keywords:
Diffusion
Heat of adsorption
Metal-organic frameworks
Hydrogen
Loading dependence

ABSTRACT

Molecular dynamics simulations of H_2 at 243 K in NU-100, UiO-68, and IRMOF-16 with zero, one, three, and six Mg alkoxide functional groups per linker were performed, revealing interesting behavior of the Maxwell–Stefan (M–S) diffusivity in these systems. A strong relationship between the isosteric heat of adsorption and the M–S diffusivity was found, with the M–S diffusivity decreasing exponentially with increasing heat of adsorption. The insights obtained may be valuable for future studies of diffusion and gas storage in nanoporous materials with strongly interacting functional groups.

1. Introduction

Metal-organic frameworks, or MOFs, are a novel class of porous, crystalline materials comprised of metal nodes and organic linkers. Because these building blocks can be combined in a modular fashion, it is possible to tailor MOFs for specific applications [1–6]. The great diversity in building blocks combined with large surface areas, large pore volumes, and the opportunity to introduce chemical functionalities within the structures make these a very exciting class of materials [7–13]. Hence, MOFs have been studied for a great variety of applications including catalysis, separations, and gas storage [6,14–26].

How well these materials perform in these applications often depends critically on the adsorption and diffusion characteristics of guest molecules adsorbed in the MOF pores. Adsorption and diffusion behaviors are dictated by many factors, including the pore size, topology, and heat of adsorption [27,28]. At low loadings, the heat of adsorption is a measure of the adsorbate/adsorbent interactions. While higher heats of adsorption are often desirable to improve of the adsorption characteristics of the material, they increase the 'sticking tendency' of the adsorbates and therefore decrease their mobility. Clearly, the relationship between the heat of adsorption and the diffusion behavior has important consequences on the usage of these materials for particular applications. Therefore, a fundamental understanding of the relationship between the heat of adsorption and diffusion is needed [27–29].

In this work, we have focused on hydrogen storage as a particular application of interest. Hydrogen storage is an important technological problem that must be solved for further implementation of fuel cell vehicles [30,31]. Thanks to the attractive features of MOFs already mentioned, they have been proposed as a possible solution [14,20,22]. Although MOFs perform very well at cryogenic temperatures [32–35], they do not adsorb enough hydrogen near room temperature due to low heats of adsorption [14]. Computational studies have suggested that a promising strategy to increase the heats of adsorption is functionalizing the linkers of the MOFs with Mg alkoxides [36–38], which display favorable interaction between the positive charge of the metal cation and the H_2 quadrupole [37,39–43]. Diffusivity studies are important to assess the loading and discharge kinetics of hydrogen molecules, which are related to the time it would take to fill and empty a tank packed with these materials in a hydrogen-powered vehicle.

In previous work [44], we calculated self, corrected, and transport diffusivities of hydrogen molecules at 243 K in NU-100 [35] and UiO-68 [45] with various numbers of alkoxide sites. We found that H_2 diffusivity values are large in all structures and mass transfer should be fast for hydrogen storage applications. In this study, we seek to elucidate the interesting behavior of the Maxwell–Stefan (M–S) diffusivity as a function of H_2 loading at 243 K exhibited by NU-100, UiO-68, and IRMOF-16 functionalized with Mg alkoxides. We utilize the theoretical framework provided by Krishna and van Baten, which demonstrates the Maxwell–Stefan diffusivity is influenced by the inverse thermodynamic correction factor and the isosteric heat of adsorption [27,28].

* Corresponding authors. Tel.: +1 847 467 2977 (R.Q. Snurr).
E-mail addresses: R.Krishna@uva.nl (R. Krishna), snurr@northwestern.edu (R.Q. Snurr).

1387-1811/$ - see front matter © 2013 Elsevier Inc. All rights reserved.
http://dx.doi.org/10.1016/j.micromeso.2013.10.031

2. Simulation details

The M–S diffusivities for NU-100 and UiO-68 with zero, one, three, and six Mg alkoxide groups per linker were calculated by equilibrium molecular dynamics (EMD) simulations and reported previously [44]. Here, we calculated the M–S diffusivities for IRMOF-16 with zero, one, three, and six Mg alkoxide groups per linker using the same method and the same force field as in our previous work [44]. IRMOF-16 was added to this study to extend the range of topologies and pore sizes for the analysis performed in this work. Fig. 1 shows the unfunctionalized versions of NU-100, UiO-68, and IRMOF-16. All simulations were performed using our in-house code RASPA [46].

The M–S diffusivity, also called the corrected diffusivity, is calculated by tracking the mean squared displacement of the center of mass of an ensemble of molecules and is related to the collective motion of the molecules [29,47,48]. It is calculated from

$$\bar{D}_i = \lim_{t\to\infty} \frac{1}{6N_i} \frac{d}{dt} \left\langle \left(\sum_{l}^{N_i} (\vec{r}_{l,i}(t) - \vec{r}_{l,i}(0)) \right)^2 \right\rangle$$

where $Đ_i$ is the M–S diffusivity of component i, which in this case is H_2, N_i is the total number of hydrogen molecules in the system, t is time, and $\vec{r}_{l,i}t$ is the position of the lth H_2 molecule at time t. The angular brackets indicate an ensemble average.

A related, but distinct, quantity is the self-diffusivity, $D_{i,self}$, which instead tracks the mean squared displacement of *individual* molecules. It is calculated from

$$D_{i,self} = \lim_{t\to\infty} \frac{1}{6N_i} \frac{d}{dt} \left\langle \sum_{l}^{N_i} (\vec{r}_{l,i}(t) - \vec{r}_{l,i}(0))^2 \right\rangle$$

The M–S diffusivity can be related to the Fick, or transport, diffusivity, D_i, through the use of the thermodynamic correction factor, Γ_i

$$D_i = \bar{D}_i \Gamma_i$$

Γ_i is defined as

$$\Gamma_i = \frac{\Theta_i}{f_i} \frac{\partial f_i}{\partial \Theta_i},$$

where f_i is the H_2 fugacity and Θ_i is the loading of H_2 molecules per unit cell of the framework. The thermodynamic correction factor can be calculated from the adsorption isotherms, which were reported for all structures of interest for this work in a previous study [38]. The adsorption isotherms were fit to a dual-site Langmuir model and the thermodynamic correction factor was calculated accordingly. Further details can be found in the Supporting Information (SI).

3. Results and analysis

Fig. 2 reports the M–S diffusivity as a function of H_2 loading for NU-100, UiO-68, and IRMOF-16 with varying degrees of Mg functionalization. For the functionalized structures, the M–S diffusivity increases with increasing H_2 loading and decreases with increasing Mg functionalization. There are two possible explanations for why the M–S diffusivity decreases with increasing number of Mg sites: a reduction of the pore size or an increase of the heat of adsorption. The reduction in pore size due to the introduction of the Mg alkoxide groups is expected to be small, but to test this quantitatively, we calculated the pore size distributions (PSDs) for all structures.

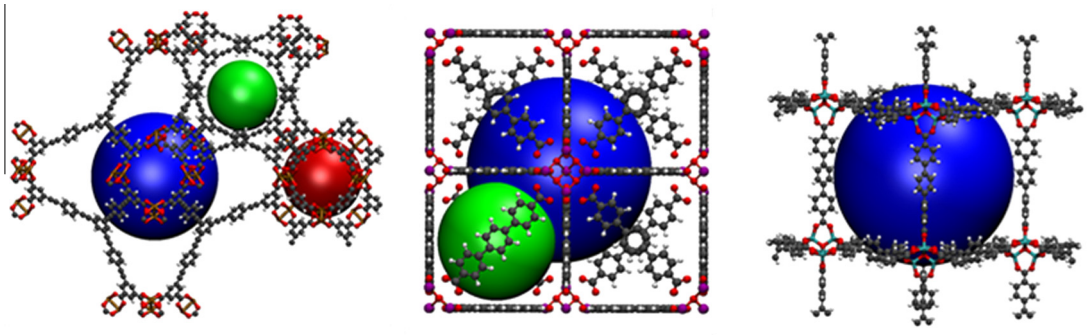

Fig. 1. NU-100 (left), UiO-68 (center), and IRMOF-16 (right). Large colored spheres are to illustrate the cavities. C = black, H = white, O = red, Cu = brown, Zn = cyan, Zr = purple. (For interpretation of the references to color in this figure legend, the reader is referred to the web version of this article.)

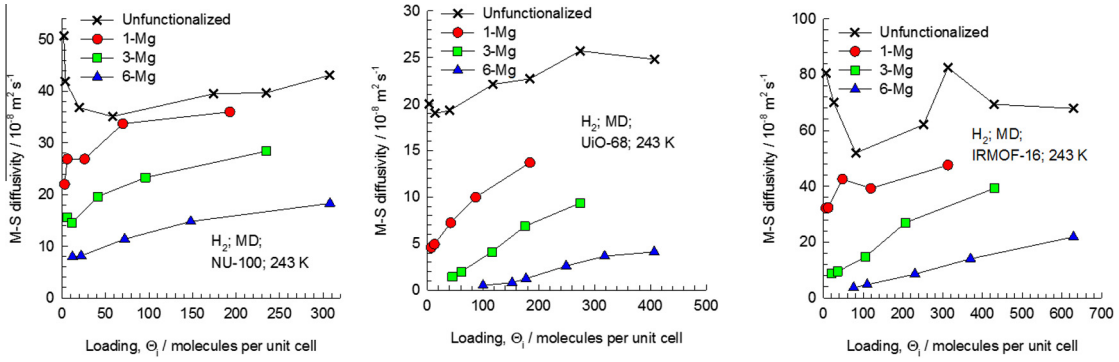

Fig. 2. The Maxwell–Stefan (M–S) diffusivity, $Đ_i$, at 243 K for H_2 in NU-100, UiO-68, and IRMOF-16 as a function of the H_2 loading.

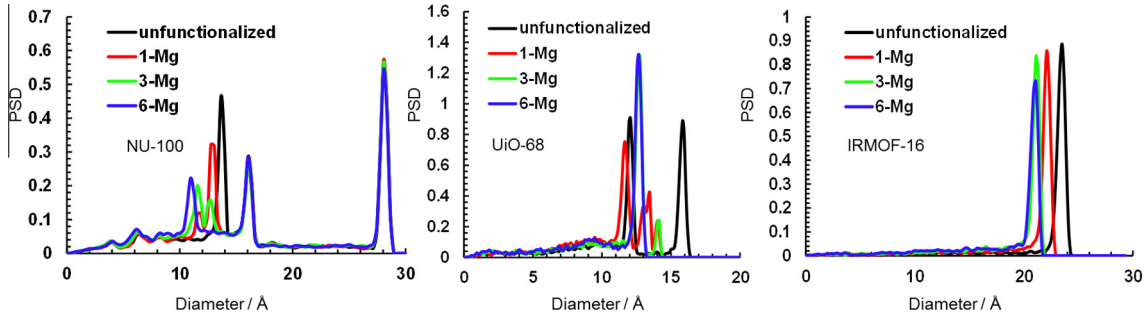

Fig. 3. Pore size distributions (PSDs) for NU-100 (left), UiO-68 (center), and IRMOF-16 (right) and their functionalized versions. Pore size distributions (PSDs) were calculated for all of the structures using the method of Gelb and Gubbins [54].

Table 1
He void fraction[a], framework density, pore volume, and pore limiting diameter[b].

MOF	Number of Mg per linker	He void fraction	Framework density (g/cm^3)	Pore limiting diameter (Å)
NU-100	Unfunctionalized	0.88	0.292	11.2
	1	0.88	0.305	10.6
	3	0.88	0.331	10.6
	6	0.87	0.372	9.5
UiO-68	Unfunctionalized	0.81	0.483	8.4
	1	0.80	0.543	8.1
	3	0.79	0.667	8.0
	6	0.78	0.847	6.9
IRMOF-16	Unfunctionalized	0.93	0.205	16.2
	1	0.92	0.233	16.2
	3	0.91	0.287	15.9
	6	0.89	0.368	14.6

[a] He void fraction was calculated using Widom insertions [52].
[b] Pore limiting diameter (PLD) was calculated using our geometric analysis program, modified from Greenfield and Theodorou [25,53].

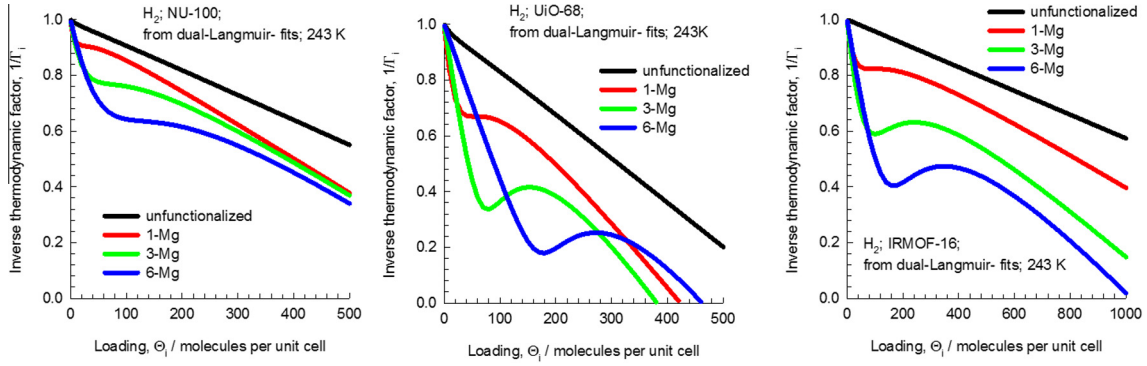

Fig. 4. The inverse thermodynamic correction factors, $1/\Gamma_i$, for NU-100, UiO-68, and IRMOF-16 at 243 K as a function of the H_2 loading.

Figs. 3 and S1 show the results. The only structure that shows significant shifts in the pore size due to functionalization is UiO-68, where the peak around 16 Å shifts to ~13 Å. NU-100 and IRMOF-16 show small shifts. Overall, the shifts in pore size are small and, therefore, cannot account for the decrease of the M–S diffusivity with increasing functionalizations.

We also calculated the He void fraction, framework density, and pore limiting diameter for all structures. The values are reported in Table 1. The only value that is significantly affected by the addition of the Mg alkoxide sites is the framework density due to the additional mass of the functional groups. The He void fraction and the PLD show little change with increasing functionalization, agreeing with the small shifts observed in the PSDs.

To further investigate the role of the Mg sites, we look at the inverse thermodynamic correction factor versus loading, which is reported in Fig. 4. For the three unfunctionalized structures there are no inflections in $1/\Gamma_i$ as a function of H_2 loading, and the simulated isotherms could be fitted with a single-site Langmuir model. For the functionalized structures, strong inflections in $1/\Gamma_i$ are found; for all three MOFs, the inflection becomes increasingly strong with increasing Mg functionalization. Similar to other sys-

Table 2
Number of Mg alkoxide sites per unit cell.

Number of Mg per linker	Number of Mg per unit cell		
	NU-100	UiO-68	IRMOF-16
1-Mg	8	24	24
3-Mg	24	72	72
6-Mg	48	144	144

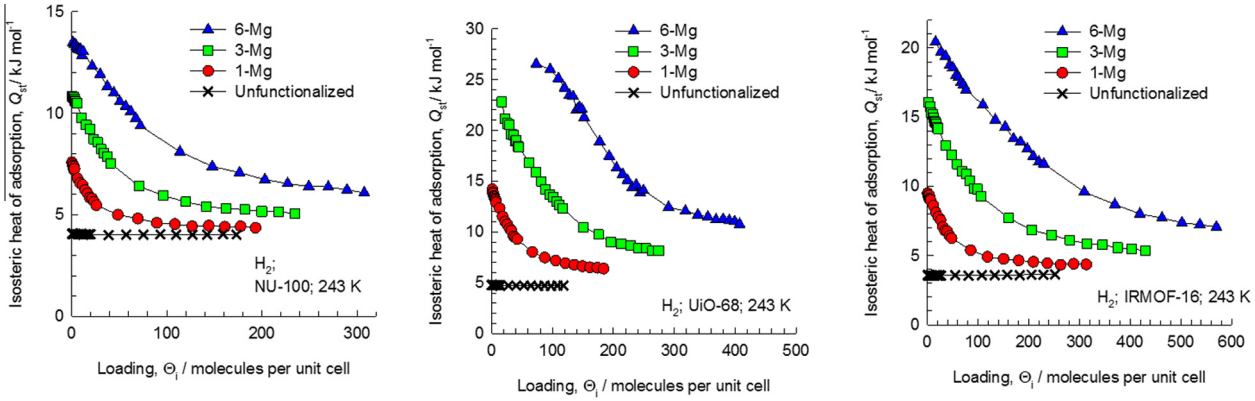

Fig. 5. The isosteric heat of adsorption, Q_{st}, for NU-100, UiO-68, and IRMOF-16 as a function of the H_2 loading at 243 K.

tems, CO_2 in Mg-MOF-74 [49] and Cu-TDPAT [50], this behavior is attributed to favorable adsorption sites within the structures, which for our case, are the Mg alkoxide sites. The simulated isotherms for H_2 in Mg-functionalized NU-100, UiO-68, and IRMOF-16 at 243 K were fitted with the dual-site Langmuir model. For the Mg-functionalized structures, the values of the saturation loading for the first site ($\Theta_{i,sat,A}$ in Tables S1–S3) correspond precisely to the number of Mg atoms per unit cell (Table 2). This number also coincides with the position of the minimum observed in $1/\Gamma_i$ reported in Fig. 4. All fit parameters can be found in the Supporting Information.

As described previously, the purpose of the Mg functionalization is to increase the heat of adsorption and thus to improve the

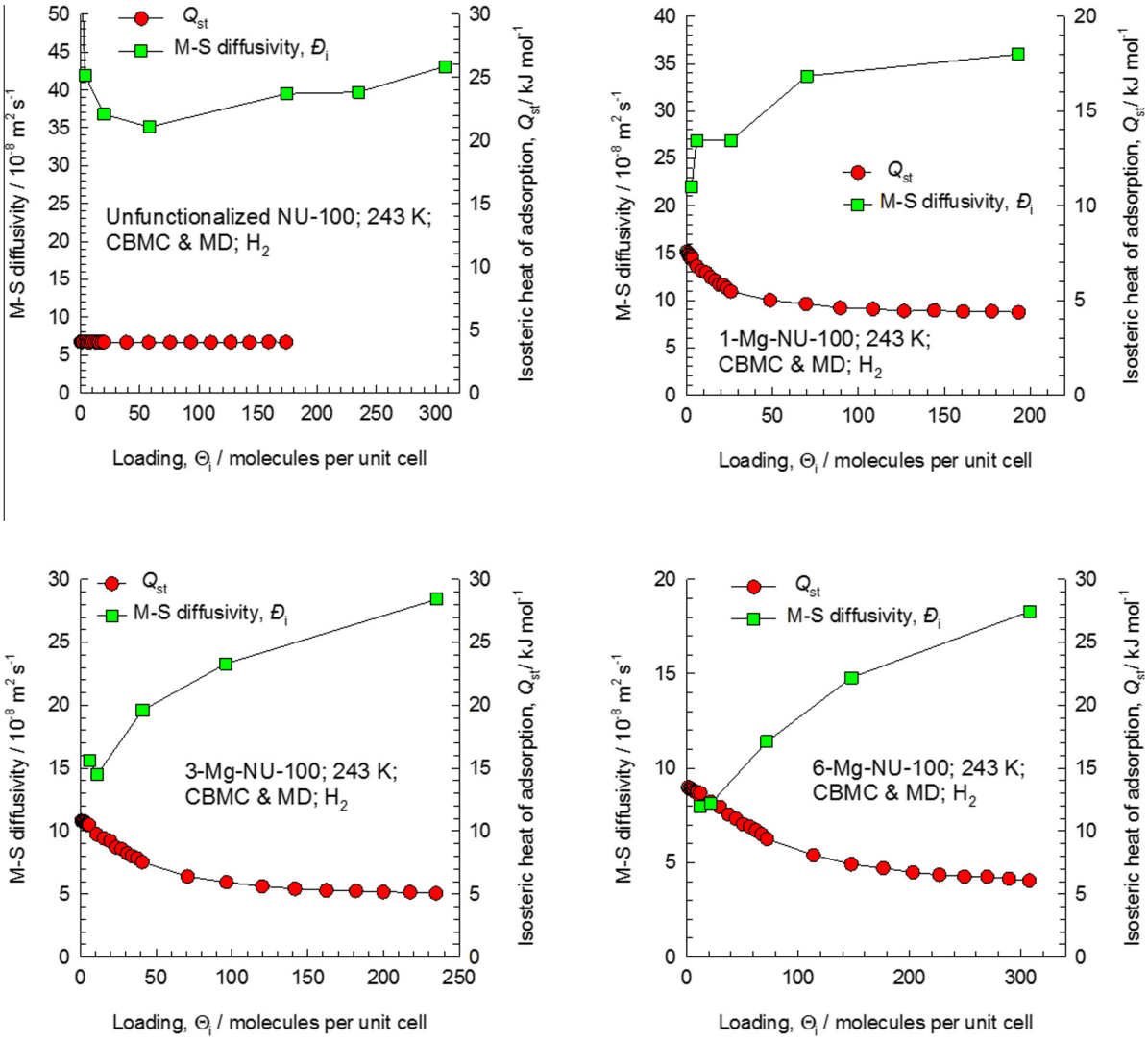

Fig. 6. Comparison of the loading dependence of the Maxwell–Stefan (M–S) diffusivity, $Đ_i$, and the isosteric heat of adsorption of H_2 in NU-100 at 243 K.

hydrogen storage properties near room temperature. Fig. 5 reports the heats of adsorption versus loading for all of the structures. As expected, the order of the curves is the opposite of that of the M–S diffusivities. In addition, similar to the inverse thermodynamic correction factors, functionalization adds curvature to the graph, while the isosteric heats of adsorption, Q_{st}, for the unfunctionalized structures remain constant for all loadings. However, for all three Mg-functionalized MOFs, the heats of adsorption decrease with increasing hydrogen loading. The reason for this is that the binding energy is strongest with the Mg atoms; furthermore, there are only a limited number of Mg atoms per unit cell.

Figs. 6–8 plot the heats of adsorption and the M–S diffusivities together as a function of loading for the three MOFs. While we expect that, qualitatively, as Q_{st} decreases, diffusivity will increase, it is striking how well the shapes of the curves mirror one another. These graphs highlight the inverse relation between the heat of adsorption and the M–S diffusivity, for the entire range of loadings. Previous publications highlighting the relation between the M–S diffusivity and Q_{st} have been restricted in their scope to diffusivity values at low loadings [27,28]. In this work, we have demonstrated that this inter-relationship holds for the entire range of loadings for three different MOFs. While other systems have shown similar behavior, in this system we were able to increase the heat of adsorption systematically, by increasing the Mg functionalization, while keeping everything else constant (pore size, pore shape, etc.).

Finally, Fig. 9 reports the M–S diffusivity versus the heat of adsorption. The unfunctionalized structures are all clustered since the heat of adsorption for these structures stays constant as a function of hydrogen loading. However, for all functionalized structures, the M–S diffusivity decays exponentially with increasing heat of adsorption. This trend can be described by an Eyring equation [51]

$$\bar{D}_i = \bar{D}_i(0)\exp\left(-a\frac{Q_{st}}{RT}\right),$$

where $Đ_i(0)$ is the M–S diffusivity in the limit of small binding energy, a is a fitting constant, R is the universal gas constant, and T is temperature. This model implies that a higher heat of adsorption increases the sticking tendency of the adsorbates, therefore decreasing the diffusivity. These results agree well with data for several other host/guest combinations collected by Krishna and van Baten [27,28].

The MD simulated data for NU-100, UiO-68, and IRMOF-16 were fitted using the equation above (Table S4). From the fits, we note that the constant a is practically the same for all three MOFs. However, the $Đ_i(0)$ values vary significantly. The values of $Đ_i(0)$ for NU-100, UiO-68, and IRMOF-16 are, respectively, 7.9×10^{-7},

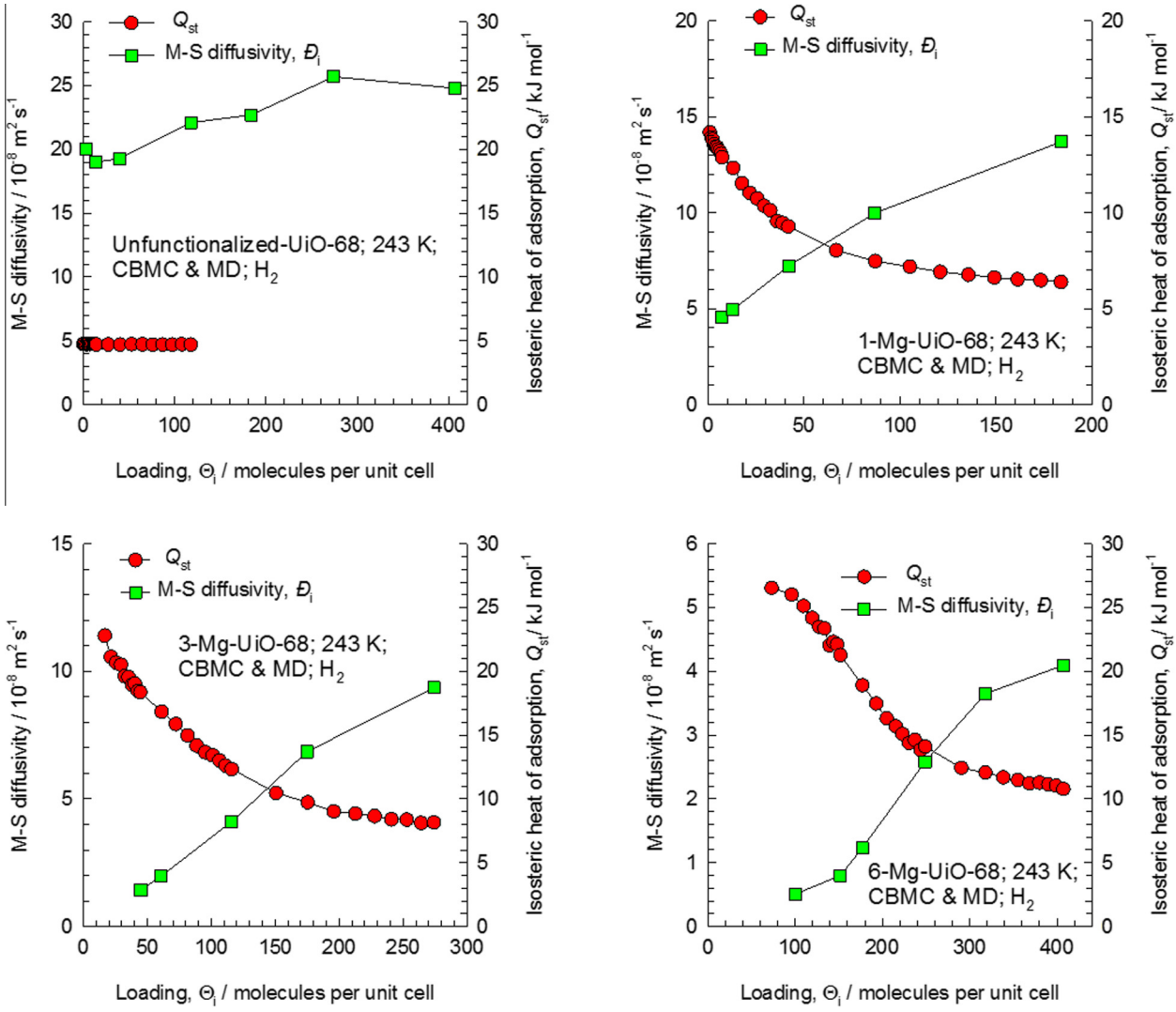

Fig. 7. Comparison of the loading dependence of the Maxwell–Stefan (M–S) diffusivity, $Đ_i$, and the isosteric heat of adsorption of H_2 in UiO-68 at 243 K.

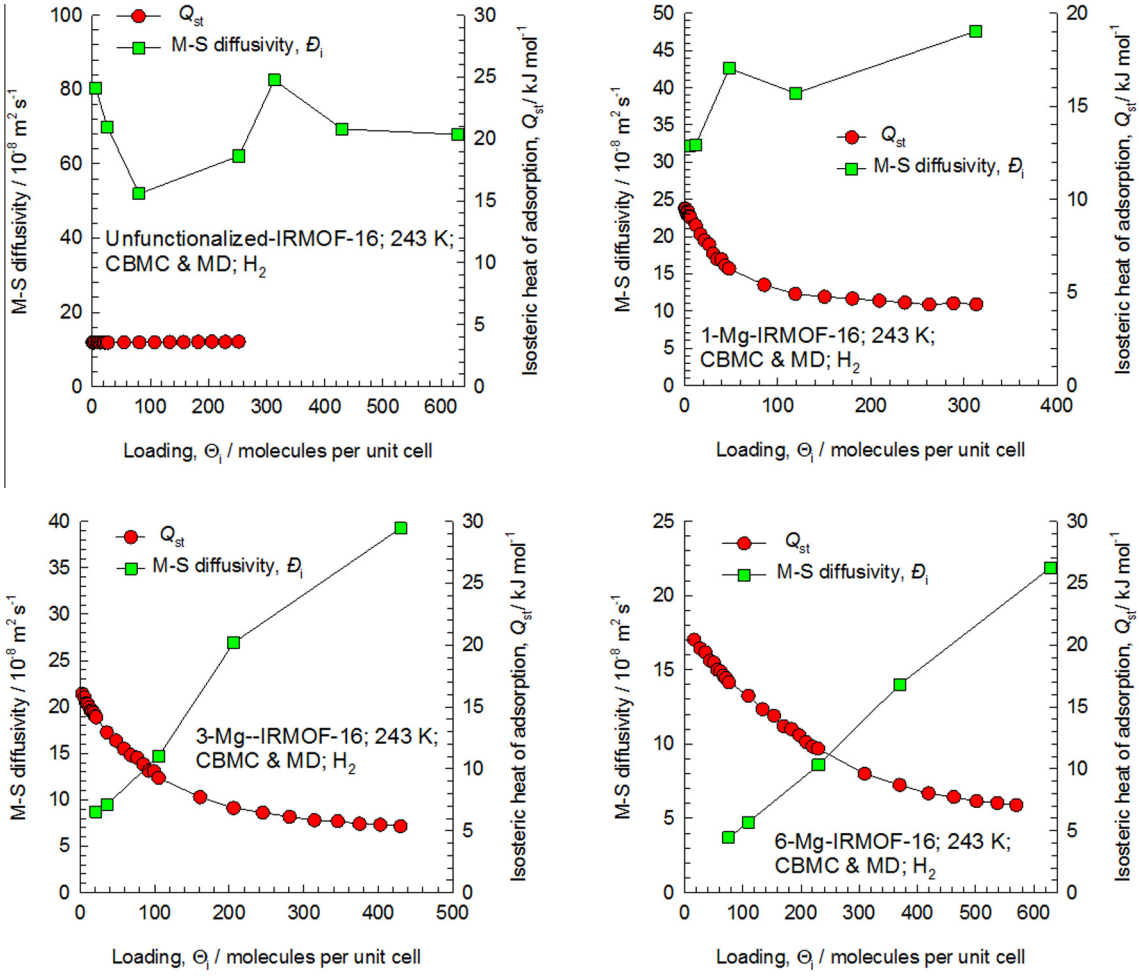

Fig. 8. Comparison of the loading dependence of the Maxwell–Stefan (M–S) diffusivity, $Đ_i$, and the isosteric heat of adsorption of H_2 in IRMOF-16 at 243 K.

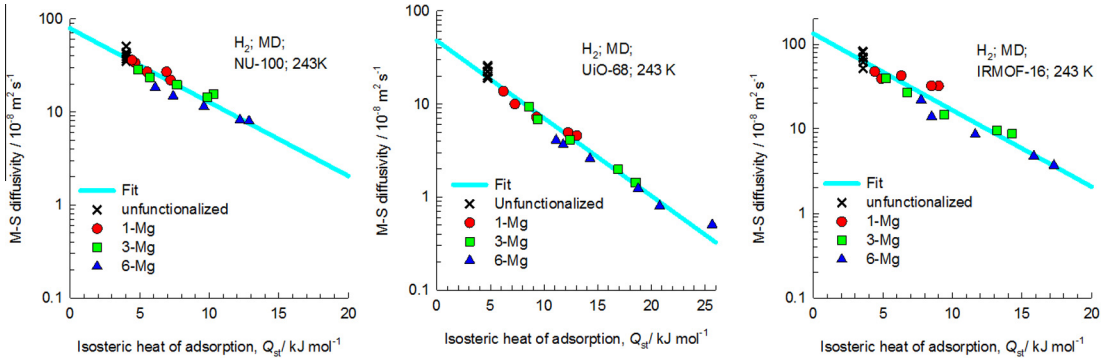

Fig. 9. M-S diffusivity, $Đ_i$, of H_2 in NU-100, UiO-68, and IRMOF-16 as a function of the isosteric heat of adsorption, Q_{st}.

4.8×10^{-7}, and 13.3×10^{-7} m^2 s^{-1}. If diffusion is limited by motion through the smallest constrictions of the pore network, we might expect $Đ_i(0)$ to correlate with the pore limiting diameters. We calculated the pore limiting diameters for NU-100, UiO-68, and IRMOF-16 to be 11.2 Å, 8.4 Å, and 16.2 Å, respectively, (Table 1), and indeed there is a correlation between these values and the values of $Đ_i(0)$ for the three materials.

4. Conclusions

In this study, we sought to elucidate the relationship between the heat of adsorption and the diffusion coefficient in porous materials with strong adsorption sites. We used as a platform the diffusion of H_2 in the MOFs NU-100, UiO-68, and IRMOF-16 functionalized with zero, one, three, and six Mg alkoxides per linker. We found that the inverse thermodynamic correction factor has a minimum when the number of adsorbed hydrogen molecules equals the number of Mg alkoxides per unit cell for all cases, reflecting preferential adsorption at the Mg sites. We also found that the shapes of the Maxwell–Stefan diffusivity and heat of adsorption curves mirror each other when plotted against the loading of hydrogen, further highlighting the relationship between the heat of adsorption and the M–S diffusivity. Finally, we showed that the M–S diffusivity decreases exponentially with increasing heat of

adsorption. This study will be helpful for other studies of hydrogen storage in MOFs, where the introduction of chemical functionalities is a necessity to improve the performance near room temperature. In addition, the lessons learned in this study can be applied to diffusion in other host/guest systems.

Acknowledgments

This work was supported by the Department of Energy (DE-FG02-08ER15967) and a National Science Foundation Graduate Research Fellowship (Grant No. DGE-0824162). Some of the calculations were performed on the National Energy Research Scientific Computing Center's Carver cluster.

Appendix A. Supplementary data

Supplementary data associated with this article can be found, in the online version, at http://dx.doi.org/10.1016/j.micromeso.2013.10.031.

References

[1] M. Eddaoudi, D.B. Moler, H. Li, B. Chen, T.M. Reineke, M. O'Keeffe, O.M. Yaghi, Acc. Chem. Res. 34 (2001) 319–330.
[2] J.L.C. Rowsell, O.M. Yaghi, Microporous Mesoporous Mater. 73 (2004) 3–14.
[3] S. Kitagawa, R. Kitaura, S.I. Noro, Angew. Chem. Int. Ed. 43 (2004) 2334–2375.
[4] G. Férey, Chem. Soc. Rev. 37 (2008) 191.
[5] S. Horike, S. Shimomura, S. Kitagawa, Nature Chem. 1 (2009) 695–704.
[6] J. Lee, O.K. Farha, J. Roberts, K.A. Scheidt, S.T. Nguyen, J.T. Hupp, Chem. Soc. Rev. 38 (2009) 1450–1459.
[7] B. Arstad, H. Fjellvåg, K. Kongshaug, O. Swang, R. Blom, Adsorption 14 (2008) 755–762.
[8] K.L. Mulfort, O.K. Farha, C.L. Stern, A.A. Sarjeant, J.T. Hupp, J. Am. Chem. Soc. 131 (2009) 3866.
[9] D. Himsl, D. Wallacher, M. Hartmann, Angew. Chem. Int. Ed. 48 (2009) 4639.
[10] C. Volkringer, T. Loiseau, N. Guillou, G.R. Férey, M. Haouas, F. Taulelle, E. Elkaim, N. Stock, Inorg. Chem. 49 (2010) 9852–9862.
[11] O.K. Farha, I. Eryazici, N.C. Jeong, B.G. Hauser, C.E. Wilmer, A.A. Sarjeant, R.Q. Snurr, S.T. Nguyen, A.Ö. Yazaydın, J.T. Hupp, J. Am. Chem. Soc. 134 (2012) 15016–15021.
[12] C.E. Wilmer, M. Leaf, C.Y. Lee, O.K. Farha, B.G. Hauser, J.T. Hupp, R.Q. Snurr, Nature Chem. (2012) 83–89.
[13] L. Sarkisov, Adv. Mater. 24 (2012) 3130–3133.
[14] J.L.C. Rowsell, O.M. Yaghi, Angew. Chem. Int. Ed. 44 (2005) 4670–4679.
[15] R.E. Morris, P.S. Wheatley, Angew. Chem. Int. Ed. 47 (2008) 4966–4981.
[16] J.-R. Li, R.J. Kuppler, H.-C. Zhou, Chem. Soc. Rev. 38 (2009) 1477–1504.
[17] D. Farrusseng, S. Aguado, C. Pinel, Angew. Chem. Int. Ed. 48 (2009) 7502–7513.
[18] A.Ö. Yazaydin, R.Q. Snurr, T.H. Park, K. Koh, J. Liu, M.D. LeVan, A.I. Benin, P. Jakubczak, M. Lanuza, D.B. Galloway, J.J. Low, R.R. Willis, J. Am. Chem. Soc. 131 (2009) 18198–18199.
[19] A.U. Czaja, N. Trukhan, U. Muller, Chem. Soc. Rev. 38 (2009) 1284–1293.
[20] L.J. Murray, M. Dinca, J.R. Long, Chem. Soc. Rev. 38 (2009) 1294–1314.
[21] A. Corma, H. Garcia, F. Llabrés i Xamena, Chem. Rev. 110 (2010) 4606–4655.
[22] M.P. Suh, H.J. Park, T.K. Prasad, D.-W. Lim, Chem. Rev. 112 (2011) 782–835.
[23] J.-R. Li, Y. Ma, M.C. McCarthy, J. Sculley, J. Yu, H.-K. Jeong, P.B. Balbuena, H.-C. Zhou, Coord. Chem. Rev. 255 (2011) 1791–1823.
[24] J.-R. Li, J. Sculley, H.-C. Zhou, Chem. Rev. 112 (2011) 869–932.
[25] B.J. Sikora, C.E. Wilmer, M.L. Greenfield, R.Q. Snurr, Chem. Sci. 3 (2012) 2217–2223.
[26] C.E. Wilmer, O.K. Farha, Y.-S. Bae, J.T. Hupp, R.Q. Snurr, Energy Environ. Sci. 5 (2012) 9849–9856.
[27] R. Krishna, J.M. van Baten, J. Phys. Chem. C 116 (2012) 23556–23568.
[28] R. Krishna, J.M. van Baten, Phys. Chem. Chem. Phys. 15 (2013) 7994–8016.
[29] R. Krishna, Chem. Soc. Rev. 41 (2012) 3099–3118.
[30] D.O.E. U.S., Energy efficiency and renewable energy, <http://www1.eere.energy.gov/hydrogenandfuelcells/storage/current_technology.html>, 2013 (accessed March 2013).
[31] D.O.E. U.S., DOE Targets for onboard hydrogen storage systems for light-duty vehicles, <http://www1.eere.energy.gov/hydrogenandfuelcells/storage/pdfs/targets_onboard_hydro_storage.pdf>, 2013 (accessed March 2013).
[32] D. Fairen-Jimenez, Y.J. Colón, O.K. Farha, Y.-S. Bae, J.T. Hupp, R.Q. Snurr, Chem. Comm. 48 (2012) 10496–10498.
[33] S.S. Kaye, A. Dailly, O.M. Yaghi, J.R. Long, J. Am. Chem. Soc. 129 (2007) 14176–14177.
[34] M. Fischer, F. Hoffmann, M. Fröba, Chem. Phys. Chem. 10 (2009) 2647–2657.
[35] O.K. Farha, A.O. Yazaydin, I. Eryazici, C.D. Malliakas, B.G. Hauser, M.G. Kanatzidis, S.T. Nguyen, R.Q. Snurr, J.T. Hupp, Nature Chem. 2 (2010) 944–948.
[36] T. Stergiannakos, E. Tylianakis, E. Klontzas, G.E. Froudakis, J. Phys. Chem. C 114 (2010) 16855–16858.
[37] R.B. Getman, J.H. Miller, K. Wang, R.Q. Snurr, J. Phys. Chem. C 115 (2011) 2066–2075.
[38] S.K. Brand, Y.J. Colón, R.B. Getman, R.Q. Snurr, Microporous Mesoporous Mater. 171 (2013) 103–109.
[39] Q. Yang, C. Zhong, J. Phys. Chem. B 109 (2005) (1864) 11862–11864.
[40] R.C. Lochan, M. Head-Gordon, Phys. Chem. Chem. Phys. 8 (2006) 1357–1370.
[41] Y.Y. Sun, Y.-H. Kim, S.B. Zhang, J. Am. Chem. Soc. 129 (2007) 12606–12607.
[42] R.C. Lochan, R.Z. Khaliullin, M. Head-Gordon, Inorg. Chem. 47 (2008) 4032–4044.
[43] M. Dinca, J.R. Long, Angew. Chem. Int. Ed. 47 (2008).
[44] Y.J. Colón, S.K. Brand, R.Q. Snurr, Chem. Phys. Lett. 577 (2013) 76–81.
[45] J.H. Cavka, S. Jakobsen, U. Olsbye, N. Guillou, C. Lamberti, S. Bordiga, K.P. Lillerud, J. Am. Chem. Soc. 130 (2008) 13850–13851.
[46] D. Dubbeldam, S. Calero, D.E. Ellis, R.Q. Snurr, RASPA, Northwestern University, Evanston, IL, 2008.
[47] E.J. Maginn, A.T. Bell, D.N. Theodorou, J. Phys. Chem. 97 (1993) 4173–4181.
[48] D. Dubbeldam, R.Q. Snurr, Mol. Simulat. 33 (2007) 305–325.
[49] J.A. Mason, K. Sumida, Z.R. Herm, R. Krishna, J.R. Long, Energy Environ. Sci. 4 (2011) 3030–3040.
[50] H. Wu, K. Yao, Y. Zhu, B. Li, Z. Shi, R. Krishna, J. Li, J. Phys. Chem. C 116 (2012) 16609–16618.
[51] J. Xiao, J. Wei, Chem. Eng. Sci. 47 (1992) 1123–1141.
[52] A.L. Myers, P.A. Monson, Langmuir 18 (2002) 10261.
[53] M.L. Greenfield, D.N. Theodorou, Macromolecules 26 (1993) 5461–5472.
[54] L.D. Gelb, K.E. Gubbins, Langmuir 15 (1998) 305–308.

Supporting Information (SI) to accompany:

Strong influence of the H_2 binding energy on the Maxwell-Stefan diffusivity in NU-100, UiO-68, and IRMOF-16

Yamil J. Colón[1], Rajamani Krishna[2]*, and Randall Q. Snurr[1]*

[1]Department of Chemical and Biological Engineering

Northwestern University, 2145 Sheridan Road, Evanston, IL 60208, USA

[2]Van 't Hoff Institute for Molecular Sciences, University of Amsterdam, Science Park 904,

1098 XH Amsterdam, The Netherlands

*To whom correspondence should be addressed.

E-mail: R.Krishna@uva.nl, snurr@northwestern.edu

1. CBMC simulated H_2 isotherms and thermodynamic correction factors

For the three unfunctionalized frameworks, the CBMC simulated isotherms at 243 K [1] could be fitted with a single-site Langmuir model

$$\Theta_i = \Theta_{i,sat} \frac{b_{i,A} f_i}{1 + b_{i,A} f_i} \tag{1}$$

For the functionalized structures, the CBMC simulated isotherms for H_2 in Mg-functionalized NU-100, UiO-68, and IRMOF-16 at 243 K [1] were fitted with the dual-site Langmuir model

$$\Theta_i = \Theta_{i,A,sat} \frac{b_{i,A} f_i}{1 + b_{i,A} f_i} + \Theta_{i,B,sat} \frac{b_{i,B} f_i}{1 + b_{i,B} f_i} \tag{2}$$

The fit parameters are summarized in Tables S1, S2, and S3.

Table S1. Dual-site Langmuir parameters for adsorption of H_2 in NU-100 at 243 K.

	$\Theta_{i,sat,A}$ molecules uc^{-1}	$b_{i,A}$ Pa^{-1}	$\Theta_{i,sat,B}$ molecules uc^{-1}	$b_{i,B}$ Pa^{-1}
NU-100 (unfunctionalized)	1120	1.79×10^{-8}		
1-Mg-NU-100	8	1.18×10^{-6}	960	2.33×10^{-8}
3-Mg-NU-100	24	1.31×10^{-6}	722	4×10^{-8}
6-Mg-NU-100	48	2.01×10^{-6}	662	6.3×10^{-8}

Table S2. Dual-site Langmuir parameters for adsorption of H_2 in UiO-68 at 243 K.

	$\Theta_{i,sat,A}$ molecules uc^{-1}	$b_{i,A}$ Pa^{-1}	$\Theta_{i,sat,B}$ molecules uc^{-1}	$b_{i,B}$ Pa^{-1}
UiO-68 (unfunctionalized)	624	2.29×10^{-8}		
1-Mg-UiO-68	24	2.48×10^{-6}	402	6.45×10^{-8}
3-Mg-UiO-68	72	1.51×10^{-5}	314	1.68×10^{-7}
6-Mg-UiO-68	144	1×10^{-4}	292	5.9×10^{-7}

Table S3. Dual-site Langmuir parameters for adsorption of H_2 in IRMOF-16 at 243 K.

	$\Theta_{i,sat,A}$ molecules uc^{-1}	$b_{i,A}$ Pa^{-1}	$\Theta_{i,sat,B}$ molecules uc^{-1}	$b_{i,B}$ Pa^{-1}
IRMOF-16 (unfunctionalized)	2346	1.2×10^{-8}		
1-Mg-IRMOF-16	24	1.24×10^{-6}	1643	2.15×10^{-8}
3-Mg-IRMOF-16	72	3.03×10^{-6}	1104	4.81×10^{-8}
6-Mg-IRMOF-16	144	9.25×10^{-6}	876	1.2×10^{-7}

The thermodynamic correction factors, Γ_i, defined by

$$\Gamma_i \equiv \frac{\Theta_i}{f_i}\frac{\partial f_i}{\partial \Theta_i}, \qquad (3)$$

were determined by analytic differentiation of the isotherm fits (2). Figure 4 presents the calculated *inverse* thermodynamic correction factors, $1/\Gamma_i$, for NU-100, UiO-68, and IRMOF-16 as a function of the H_2 loading at 243 K.

2. Dependence of $Đ_i$ on isosteric heats of adsorption, Q_{st}

We note that for all three structures the M-S diffusivity of H_2 decays exponentially with increasing heat of adsorption, in conformity with the model

$$Đ_i = Đ_i(0)\exp\left(-a\frac{Q_{st}}{RT}\right) \tag{4}$$

where $Đ_i(0)$ is the M-S diffusivity in the limit of vanishingly small binding energy.

The MD simulated data for NU-100, UiO-68, and IRMOF-16 were fitted using equation (4); the fit parameters are provided in Table S4.

Table S4. Fitting of the dependence of the Maxwell-Stefan diffusivity on the isosteric heat of adsorption.

NU-100	$Đ_i = 7.9\times10^{-7}\exp\left(-0.37\frac{Q_{st}}{RT}\right)$
UiO-68	$Đ_i = 4.8\times10^{-7}\exp\left(-0.39\frac{Q_{st}}{RT}\right)$
IRMOF-16	$Đ_i = 13.3\times10^{-7}\exp\left(-0.42\frac{Q_{st}}{RT}\right)$

3. Pore size distributions

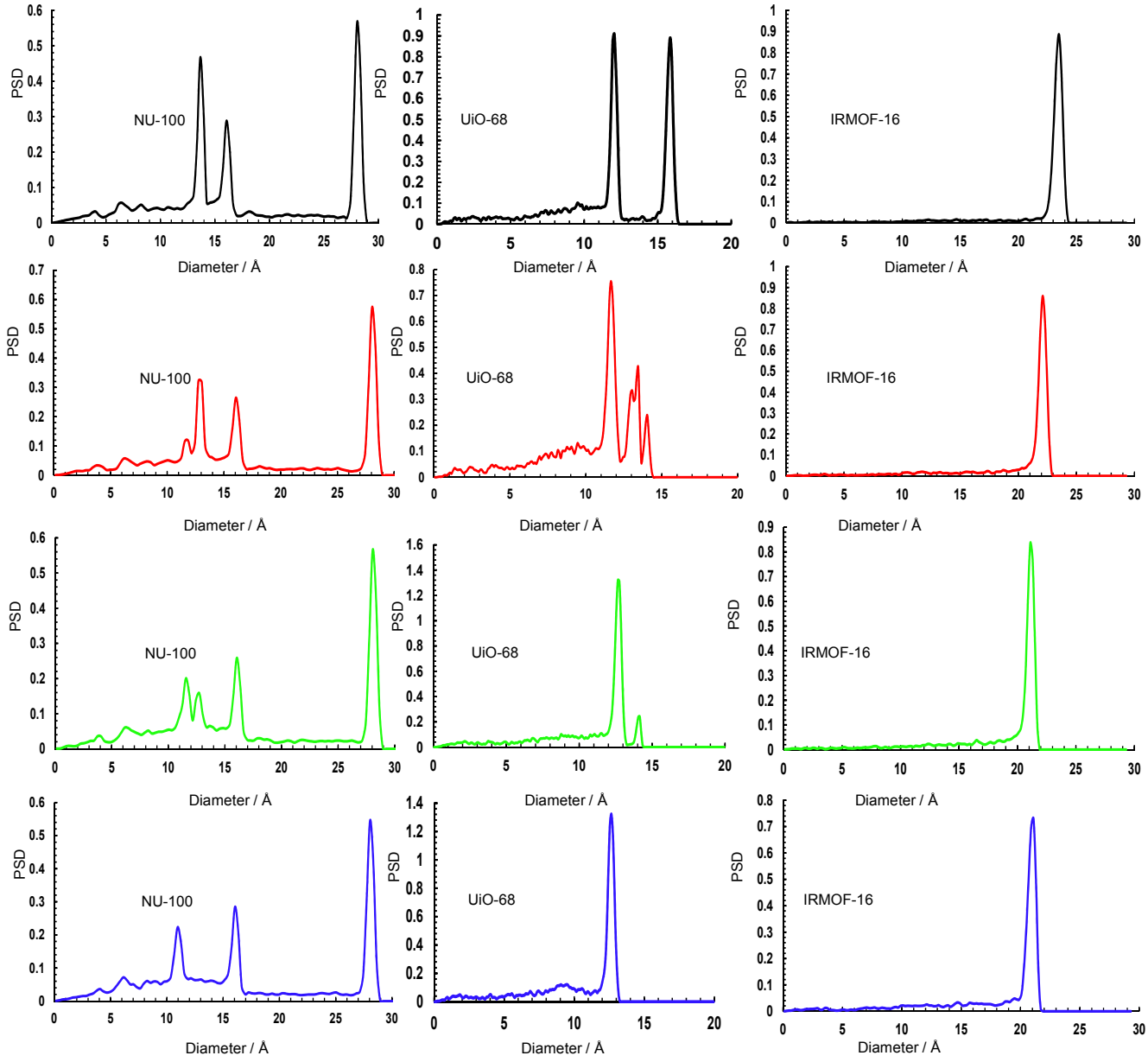

Figure S1. Pore size distributions (PSDs) for NU-100 (left), UiO-68 (center), and IRMOF-16 (right) with zero (top), one (second row), three (third row), and six (bottom) Mg alkoxides per linker.

4. Notation

a	constant defined in equation (4), dimensionless
b_i	Langmuir constant, Pa^{-1}
$Đ_i$	Maxwell-Stefan diffusivity, $m^2\ s^{-1}$
$Đ_i(0)$	Maxwell-Stefan diffusivity for $Q_{st} = 0$, $m^2\ s^{-1}$
Γ_i	thermodynamic correction factor, dimensionless
f_i	fugacity, Pa
c_i	concentration, molecules per unit cell
Q_{st}	isosteric heat of adsorption, J mol^{-1}
R	gas constant, 8.314 J mol^{-1} K^{-1}
T	absolute temperature, K

Greek letters

Θ_i	loading of species *i*, molecules per unit cell
$\Theta_{i,sat}$	saturation loading of species *i*, molecules per unit cell

5. References

[1] S.K. Brand, Y.J. Colón, R.B. Getman, R.Q. Snurr, Microporous Mesoporous Mater., 171 (2013) 103-109.